ANNUAL REVIEWS

Annual Review of Biochemistry

The Activation Mechanism of the Insulin Receptor: A Structural Perspective

Eunhee Choi[1] and Xiao-Chen Bai[2]

[1]Department of Pathology and Cell Biology, Vagelos College of Physicians and Surgeons, Columbia University, New York, New York, USA; email: EC3477@cumc.columbia.edu

[2]Department of Biophysics, University of Texas Southwestern Medical Center, Dallas, Texas, USA; email: Xiaochen.Bai@UTSouthwestern.edu

Annu. Rev. Biochem. 2023. 92:247–72

First published as a Review in Advance on March 31, 2023

The *Annual Review of Biochemistry* is online at biochem.annualreviews.org

https://doi.org/10.1146/annurev-biochem-052521-033250

Keywords

insulin receptor, insulin, cryo-EM, activation mechanism, insulin-binding site 1, insulin-binding site 2

Abstract

The insulin receptor (IR) is a type II receptor tyrosine kinase that plays essential roles in metabolism, growth, and proliferation. Dysregulation of IR signaling is linked to many human diseases, such as diabetes and cancers. The resolution revolution in cryo–electron microscopy has led to the determination of several structures of IR with different numbers of bound insulin molecules in recent years, which have tremendously improved our understanding of how IR is activated by insulin. Here, we review the insulin-induced activation mechanism of IR, including (*a*) the detailed binding modes and functions of insulin at site 1 and site 2 and (*b*) the insulin-induced structural transitions that are required for IR activation. We highlight several other key aspects of the activation and regulation of IR signaling and discuss the remaining gaps in our understanding of the IR activation mechanism and potential avenues of future research.

Contents

1. INTRODUCTION

The discovery of insulin in 1921 is one of the most significant medical breakthroughs that changed the world (1). In the past, children and adults who developed diabetes most often died within a few years, sometimes even within a few days or weeks of their diagnosis. Since Frederick Banting and

Charles Best successfully isolated the hormone, people suffering from diabetes have been treated with insulin, and diabetes is no longer considered fatal. Insulin was believed to play a role in the enzymatic process of glucose phosphorylation for 30 years following its discovery. The concept of insulin acting to facilitate glucose uptake into cells was proposed in 1950 (2); however, how insulin initiates this process was unclear until the discovery of a membrane receptor for insulin, the insulin receptor (IR), in 1971 (3). Kahn and colleagues discovered that insulin stimulates tyrosine phosphorylation of the IR by forming an IR–insulin complex (4, 5). IR cDNAs were cloned in 1985 (6, 7), and the concept of signal transduction by receptor tyrosine kinases (RTKs) was established, making IR and aberrant RTK activation potential therapeutic targets.

In vertebrates, the IR belongs to the IR family, which consists of three type-II RTKs: IR (6, 7), insulin-like growth factor 1 receptor (IGF1R) (8), and IR-related receptor (9). The IR is derived from a single polypeptide that is posttranslationally cleaved into two subunits, α and β, which are then cross-linked by multiple disulfide bridges to form a homodimer (α2β2) (10). The extracellular domains (ECDs) of IR contain two leucine-rich repeats (L1 and L2), a cysteine-rich region (CR), and three consecutive fibronectin type III (FnIII-1, -2, and -3) domains (11) (**Figure 1*a***). The FnIII-2 domain contains a furin cleavage site. After cleavage by furin, the insulin proreceptor is converted into a mature receptor, consisting of the α and β subunits (10). The C-terminal domain of the α subunit is referred to as the α-CT motif, and it is constitutively associated with

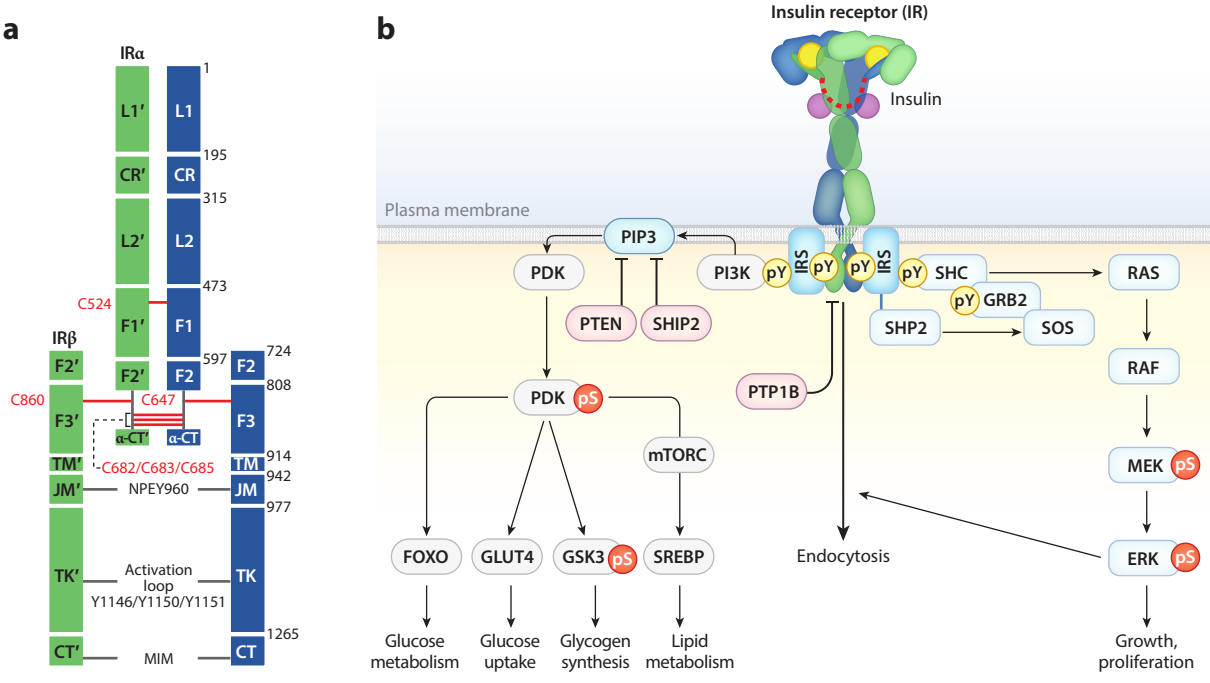

Figure 1

Structure and signaling of IR. (*a*) Schematic representation of the structure of the disulfide-linked IR. The two protomers are shown in green and blue. Disulfide bonds are shown in red. The NPEY motif, MIM, and tyrosine triplets in the activation loop are indicated. (*b*) Insulin-activated IR triggers two signaling cascades involving the PI3K–AKT and MAPK pathways. The IR undergoes endocytosis, which redistributes and terminates IR signaling. Arrows and blunt ends indicate activation and inhibition, respectively. Abbreviations: α-CT, C-terminal domain of the α subunit; CR, cysteine-rich region; CT, C-terminal region of the β subunit; F, fibronectin type III domain; IR, insulin receptor; JM, juxtamembrane; L, leucine-rich repeat; MAPK, mitogen-activated protein kinase; MIM, MAD2-interacting motif; pS, phosphor-Ser/Thr; pY, phosphor-Tyr; TK, tyrosine kinase; TM, transmembrane.

the L1 domain. The remaining β subunit passes through the cellular membrane via a single transmembrane (TM) domain that is linked to the intracellular domains (ICDs), including the juxtamembrane, tyrosine kinase, and C-terminal domains. Unlike all other RTKs, IR forms a stable dimer independent of ligand binding. The two protomers are covalently linked by multiple disulfide bonds between the FnIII-1 domains and α-CTs (12, 13) (**Figure 1*a***).

The mammalian IR exists as two isoforms: isoform A (IR-A), which lacks exon 11, and isoform B (IR-B), which includes exon 11 (6, 7, 14). Exon 11 encodes a 12-amino-acid segment in the α-CT. IR-A and IR-B bind to native insulin with similar affinity; however, the binding affinity of IR-A for IGF1 and IGF2 is significantly higher than that of IR-B (15), suggesting that the extension plays an important role in regulating the ligand-binding process and that IR-B is a more insulin-specific receptor. The molecular basis for the role of the 12-amino-acid segment in the activation of insulin-bound or IGF-bound IR is still unclear.

Most mammalian cells express IR, but its expression levels are regulated depending on cell type, developmental stage, and disease state. The main target tissues of insulin's metabolic action are liver, muscle, and adipose tissue (16–19). In the liver, insulin-activated IR promotes glycogen and triglyceride synthesis and inhibits glucose production (16, 18, 20). In muscle, insulin-activated IR promotes glucose uptake and glycogen synthesis, while in adipose tissue, insulin promotes glucose uptake and inhibits lipolysis (17, 20). Aside from controlling systemic metabolic homeostasis, IR in the brain regulates cognitive behavior, food intake, and depression (21, 22). In highly proliferative T cells, IR expression is increased, and loss of IR causes defects in proliferation and optimal immunity (23). Furthermore, IR plays a role in insulin clearance, while IR in endothelial cells transports insulin via transcytosis to the brain, muscles, and adipose tissue (24, 25). Because IR signaling affects all tissues in the body and controls diverse biological responses, IR signaling dysfunction leads to various diseases including diabetes, cancer, cardiovascular diseases, and even Alzheimer's disease.

In this review, we mainly focus on the molecular basis of insulin-dependent IR activation and discuss how binding of multiple insulin molecules to two distinct sites promotes optimal IR signaling. We also highlight key aspects of the activation and regulation of IR signaling and provide insight into the structure–function relationship of the IR. However, structural studies of the IR ICD, as well as its complex with downstream effector proteins, are not discussed here. For this topic, we refer the reader to references 26–30.

2. INSULIN-INDUCED INSULIN RECEPTOR SIGNALING

Insulin activates two main signaling pathways, the PI3K–AKT and mitogen-activated protein kinase (MAPK) pathways, through IR on the plasma membrane by forming an IR–insulin high-affinity complex (16, 31–33) (**Figure 1*b***). The binding of insulin to IR shows complex characteristics involving multiple binding events (i.e., insulin binds to two distinct sites on IR, site 1 and site 2) and negative cooperativity (34–36). Moreover, it has also been established that the binding of insulin to IR induces a large conformational change in IR that facilitates autophosphorylation and triggers downstream signaling cascades. The insulin-activated IR kinase transautophosphorylates multiple tyrosine residues in the intracellular region: phospho-Y953 (pY953) and pY960 in the juxtamembrane domain; pY1146, pY1150, and pY1151 in the activation loop of the kinase domain; and pY1316 and pY1322 in the C-terminal domain (3–7, 37, 38) (note that we use the numbering system of the mature form of human IR-A). The phosphorylated tyrosine residues provide docking sites for downstream effector and adaptor proteins, thus triggering phosphorylation-mediated signaling cascades (39) (**Figure 1*b***).

The first IR substrates (IRSs) to be discovered were a family of adaptor proteins that convert the tyrosine phosphorylation signal into a lipid kinase signal by recruiting phosphoinositide

3-kinase (PI3K) to the plasma membrane (40–45) (**Figure 1*b***). In humans, three homologous IRS proteins exist (IRS1, IRS2, and IRS4) (42). IRS1 and IRS2 are expressed widely, while the expression of IRS4 is tissue specific. The activated IR autophosphorylates a motif named NPEY960 in the juxtamembrane domain, and IRS directly binds to the NPEpY960 motif. Subsequently, the IR phosphorylates multiple tyrosine residues on IRS, which in turn recruit SH2 domain–containing downstream proteins, including PI3K. The triphosphorylated inositol produced by PI3K activates the serine/threonine kinase AKT, which initiates serine/threonine phosphorylation cascades (46, 47). Insulin-dependent metabolic processes are largely governed by the PI3K–AKT pathway (48–52). More specifically, the PI3K–AKT pathway regulates glucose uptake by glucose transporter type 4 (GLUT4) (53–56), glycogen synthesis by glycogen synthase kinase 3 (GSK3) (57, 58), protein and lipid metabolism by mammalian target of rapamycin (mTOR) (59–61), and glucose metabolism by forkhead family box O (FOXO) (62–67).

Furthermore, the insulin-activated IR recruits and phosphorylates an adaptor protein, SH3-containing protein (SHC), which can interact with the SH2/SH3 adaptor protein GRB2 (growth factor receptor bound protein 2) and guanine nucleotide exchange factor SOS (son of sevenless) (68–71) (**Figure 1*b***). The GRB2–SOS complex activates the MAPK pathway, which mainly controls cell growth and proliferation. IRSs also recruit the GRB2–SOS2 complex, contributing to activation of the MAPK pathway as well. A nonreceptor protein tyrosine phosphatase, SHP2, facilitates the activation of the MAPK pathway (72, 73). The complexities of the IR signaling pathways have been thoroughly reviewed elsewhere. We refer the reader to references that provide a more comprehensive summary of IR signaling (16, 31, 33, 74).

3. THE STRUCTURE OF THE UNLIGANDED APO INSULIN RECEPTOR

The structure of the complete ECD of IR in the unliganded, apo state was first determined at 3.8-Å resolution by X-ray crystallography in 2006 (75), and it was further improved to 3.3-Å resolution in 2016 [Protein Data Bank identifier (PDB ID): 4ZXB] (76) (**Figure 2**). These structures represent major breakthroughs in the structural biology of IR family receptors. The overall structure of IR in the unliganded, apo state displays a Λ shape (**Figure 2**). Two IR protomers, each of which adopts a 7-shaped conformation, pack tightly together through the interaction between the L1 and L2 domains of one protomer and the FnIII-2′ and FnIII-1′ domains of another. The L1 domain interacts with the FnIII-2′ domain in the middle part of the Λ, through highly complementary surfaces (**Figure 2**). The α-CT′ and the long linker between the α-CT′ and FnIII-2′ domains also contribute to this interaction. In the top region of the Λ, the L2 domain packs against the FnIII-1′ domain using a number of hydrophobic and polar residues, such as L403, H429, and Y430 (L2 domain) and L569, T571, and F572 (FnIII-1′ domain). At the same interface, the two L2 domains also make strong homotypic interactions, mainly via hydrogen bonds. With such interaction patterns, the two membrane-proximal FnIII-3 domains are separated by a long distance (**Figure 2**), which prevents the intracellular kinase domains from undergoing efficient autophosphorylation, suggesting that such a Λ-shaped structure represents the autoinhibited state of IR. It is, therefore, reasonable to imagine that a large conformational rearrangement, induced by insulin binding, is required for IR activation.

4. THE STRUCTURE OF THE LIGAND-BOUND, ACTIVE INSULIN RECEPTOR

In 2013, the first structure of insulin-bound IR was determined by X-ray crystallography, using a truncated ECD of IR that contained only the L1 and CR domains and an α-CT peptide, revealing how insulin engages site 1 of IR (PDB ID: 3W11) (77). Nevertheless, the crystallization of the

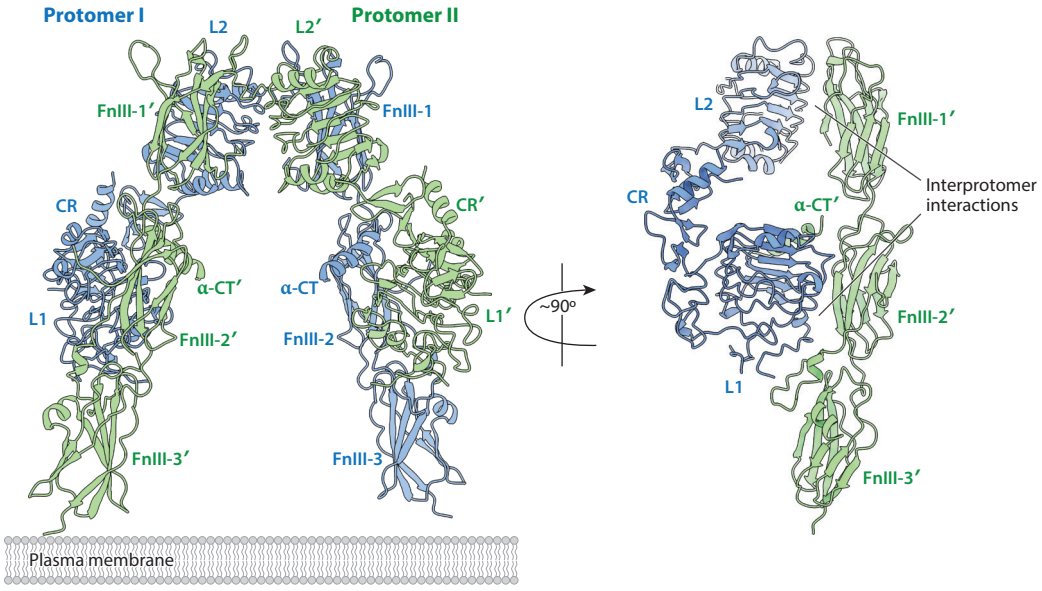

Figure 2

The X-ray crystal structure of the insulin receptor extracellular domain in the apo, unliganded state, showing a Λ-shaped conformation (Protein Data Bank identifier: 4ZXB). Abbreviations: α-CT, C-terminal domain of the α subunit; CR, cysteine-rich region; FnIII, fibronectin type III domain; L, leucine-rich repeat.

insulin-bound intact IR ECD or full-length IR is a challenge, due to the difficulties of large-scale protein purification and the nature of structural dynamics. In 2011, a combination of hardware and software advances led to the so-called resolution revolution in single-particle cryo–electron microscopy (cryo-EM) (78). Since then, cryo-EM has become the major tool for structural studies of single-pass transmembrane receptors, including IR, as it requires a much smaller amount of protein and can tolerate certain levels of impurity and structural heterogeneity (79). In 2018, two different groups determined the cryo-EM structures of the complete ECD of IR bound to insulin at approximately 4-Å resolution (80, 81). Despite some differences in construct design, these two structures of the IR ECD–insulin complex share similar structural characteristics. Specifically, upon insulin binding to IR site 1, the overall architecture of the IR changes from an autoinhibited Λ shape to a T shape. The large structural change brings the two kinase domains of the IR into close proximity, allowing efficient autophosphorylation, which leads to the activation of IR signaling.

Although these two cryo-EM structures represented another major advance in the structural studies of IR, they were both resolved at relatively low resolution, suggesting the intrinsic instability of the truncated IR ECD samples. In addition, neither of them could uncover the second insulin-binding site. As insulin binds to full-length IR more strongly than to the truncated IR ECD, structural studies of full-length IR in complex with insulin are essential for capturing the stable, fully liganded state of IR (82–84).

The cryo-EM structure of full-length IR in the presence of saturating insulin concentrations was determined at 3.2-Å resolution (1:4 IR:insulin; PDB ID: 6PXV) in 2019 (85), and the structure of the IR ECD was determined at an oversaturated insulin concentration at 4.3-Å resolution (1:28 IR:insulin; PDB ID: 6SOF) in 2020 (86) (**Figure 3*a***). To obtain sufficient full-length IR for cryo-EM analysis, several new strategies were applied during the expression and purification of

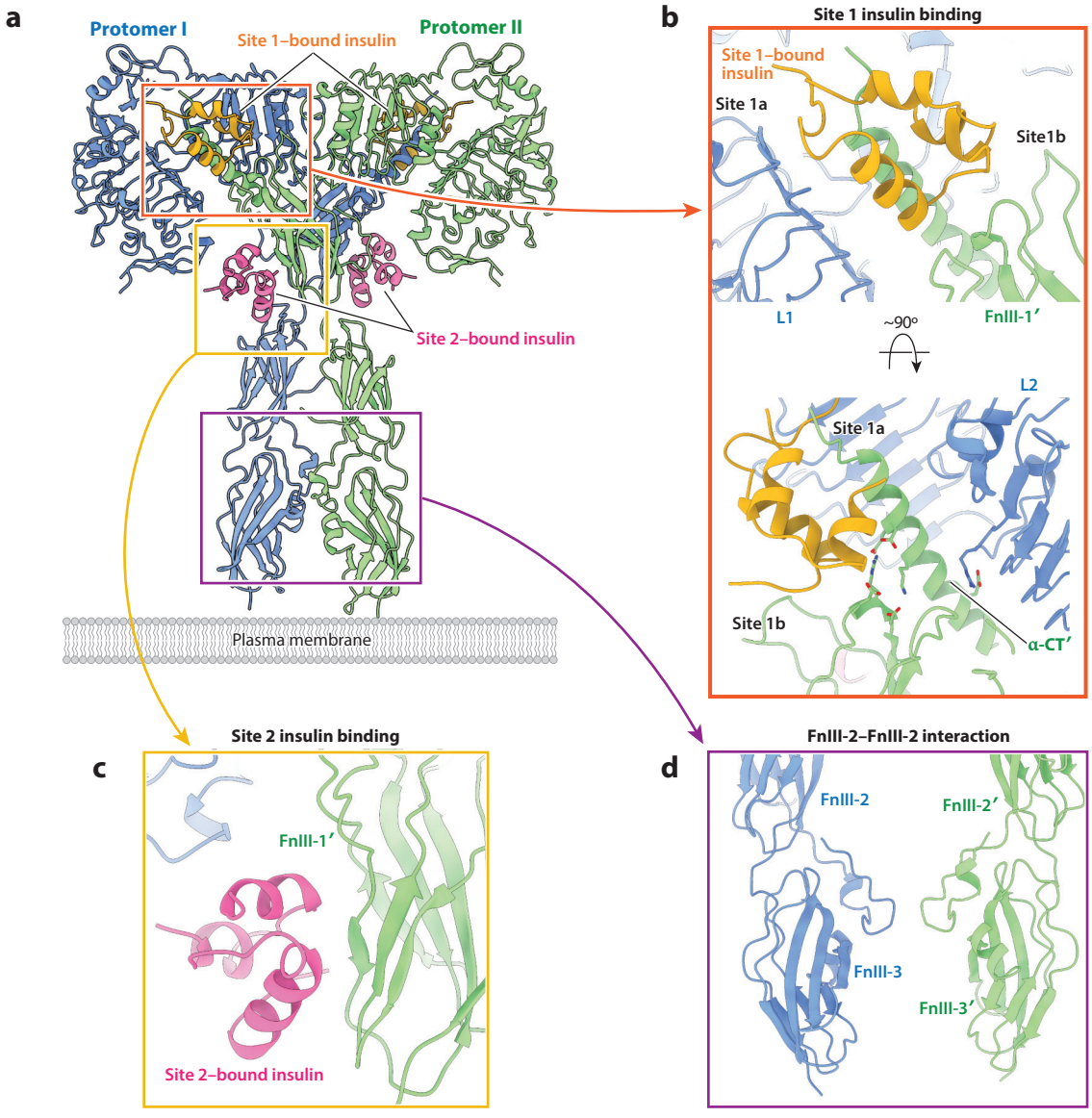

Figure 3

The cryo-EM structure of full-length IR in the active, fully liganded state, showing a T-shaped symmetric conformation (PDB ID: 6PXV). (*a*) A T-shaped IR dimer bound to 4 insulin molecules at site 1, site 1′, site 2, and site 2′. (*b*) The detailed binding mode of site 1–bound insulin in the T-shaped IR. The site 1–bound insulin cross-links the L1 of one protomer and the α-CT′ and FnIII-1′ domain of another. The α-CT′ contacts both the L2 and FnIII-1′ domains in the T-shaped IR. (*c*) The detailed binding mode of site 2–bound insulin in the T-shaped IR. Site 2–bound insulin interacts with a side surface of the FnIII-1 domain. (*d*) The homotypic FnIII-2–FnIII-2′ interaction in the T-shaped IR. Abbreviations: α-CT, C-terminal domain of the α subunit; FnIII, fibronectin type III domain; IR, insulin receptor; L, leucine-rich repeat; PDB ID, Protein Data Bank identifier.

full-length IR: (*a*) Several mutations in the IR ICD were introduced to reduce IR endocytosis (87), and (*b*) a new affinity purification approach based on the strong interaction between the T6SS effector Tse3 and its immunity protein Tsi3 was developed and applied (88). In the full-length IR–insulin complex, the dimerized TM domains of IR were resolved at the secondary structural level, showing a crossover at the N terminus of the TM helices (85). This structural observation suggests that the TM–TM interaction plays a role in stabilizing the active conformation of IR, which explains in part why the cryo-EM structure of the full-length IR–insulin complex was resolved at a higher resolution than the IR ECD–insulin complex. Strikingly, these structures reveal that IR in the presence of saturating insulin concentrations adopts a T-shaped symmetric conformation, with four insulin molecules bound at four sites (named sites 1, 1′, 2, and 2′) that are related by C2 symmetry (**Figure 3*a***). More importantly, for the first time, the binding mode between IR and site 2–bound insulin has been revealed in atomic detail, representing another major milestone in the structural biology of IR. In the next sections, we describe in detail the binding mode and the function of binding at site 1 and site 2.

5. INSULIN-BINDING SITE 1

The primary insulin-binding site of IR is composed of the L1 domain and the α-CT (namely site 1a) (**Figure 3*b***). Structural comparisons between the insulin-free and insulin-bound L1 and α-CTs reveal that insulin binding to this site induces a remarkable relocation of the α-CT relative to the L1 domain, suggesting that a certain level of flexibility in the α-CT is required for insulin binding. Strikingly, 24 of insulin's 51 residues are involved in binding to site 1a (77, 85). The residues from the A chain of insulin predominantly contact the α-CT, while the residues from the B chain of insulin interact with both the L1 domain and the α-CT, through a combination of Van der Waals and hydrogen-bonding interactions (**Figure 3*b***). As many other review papers have described insulin binding to site 1a (89, 90), we do not go into detail here. In addition to this primary interface, the site 1a–bound insulin in the T-shaped IR form simultaneous contacts the loops in the top region of the FnIII-1′ domain from the adjacent protomer (namely site 1b) (85) (**Figure 3*b***). Several residues from the B chain of insulin, including His-B5, Ser-B9, and His-B10, contribute to this interaction. In this binding mode, one insulin concurrently engages two protomers, thereby stabilizing the T-shaped active conformation of IR (**Figure 3*b***).

6. INSULIN-BINDING SITE 2

The high-resolution cryo-EM structure of full-length IR–insulin in the fully liganded state identified the location of insulin-binding site 2 in IR and revealed the detailed binding mode of insulin at site 2 (85). The newly discovered site is located at the side surface of a β-sheet in the FnIII-1 domain of IR (**Figure 3*c***). A total of 14 residues from both the A and B chains of insulin, such as Leu-A13, Glu-A17, His-B10, Glu-B13, and Leu-B17, are critical for insulin binding to site 2. As the site 2–bound insulin contacts only one surface of the T-shaped IR, it is nonessential for maintaining the active conformation (**Figure 3*c***). Nevertheless, the significance of insulin binding at site 2 in IR activation has been demonstrated by mutagenesis, binding, and cell-based assays (85, 91). Structural studies have revealed the function of insulin binding at site 2 and are discussed in Section 10.

7. RECEPTOR–RECEPTOR INTERFACES FOR MAINTAINING THE T-SHAPED ACTIVE INSULIN RECEPTOR DIMER

The cryo-EM structure of the full-length IR–insulin complex also revealed several receptor–receptor interfaces critical to the structural stability of the T-shaped IR dimer (85). Firstly, in the

top part of the T, each α-CT adopts a long α-helical conformation and contacts both the FnIII-1 domain of the same protomer and the L2′ domain of another (**Figure 3*b***). These interactions exclusively exist in the T-shaped IR dimer and are critical for maintaining the active conformation. These interfaces involve a cluster of charged residues, including E697, K703, E706, and D707 (α-CT); D496, R498, and D499 (FnIII-1 domain); and R345 (L2 domain), forming multiple salt bridges (**Figure 3*b***). Secondly, in the bottom part of the T, the two FnIII-2 domains form a homotypic interaction, further stabilizing the membrane-proximal domains of IR (**Figure 3*d***). The FnIII-2–FnIII-2′ interaction may also facilitate dimerization of the TM domains, which place the two intracellular kinase domains in optimal relative positions for autophosphorylation.

8. STRUCTURES OF THE INSULIN RECEPTOR AT SUBSATURATING INSULIN CONCENTRATIONS

In two recent studies, cryo-EM structures of a series of partially liganded full-length IRs with one or two insulin molecules bound were determined, using the insulin site-specific mutants or subsaturating insulin concentrations (92, 93) (**Figure 4*a*,*b***). The structure of full-length IR with a single insulin molecule bound assumes a Γ-shaped conformation, which is almost identical to that of full-length IGF1R with a single IGF1 molecule bound (94) (**Figure 4*a***). This single insulin is bound at one of the site 1s in the top part of the Γ and forms extensive interactions with the L1′, α-CT, and FnIII-1 domains. In the bottom part of the Γ, the unliganded L1 domain contacts both membrane-proximal domains, which further stabilizes the Γ-shaped conformation. This structural configuration places both intracellular kinase domains close together, enabling autophosphorylation to occur. Thus, the Γ-shaped IR dimer represents an (partially) active state of IR (**Figure 4*a***).

Strikingly, in response to the binding of two insulin molecules, IR predominantly adopts a *T*-shaped asymmetric conformation (∼80% of particles) (**Figure 4*b***), while only a small population of IR forms a T-shaped symmetric dimer (∼20% of particles) (92, 93). The conformation of the T-shaped IR with two insulin molecules bound at site 1s is almost identical to that of the 2:4 IR–insulin complex. In the *T*-shaped asymmetric IR, one insulin is bound at site 1 in the top part of the *T* in the same fashion as the binding of insulin to site 1 in the T-shaped symmetric IR, while another insulin is bound in the middle region of the *T*, simultaneously contacting sites 1 and 2′ from two adjacent protomers (named the hybrid site) (**Figure 4*b***). Intriguingly, the cryo-EM analyses of the full-length IR show that the hybrid site can be cross-linked and stabilized by one insulin in two different ways (92) (**Figure 4*b***): (*a*) Insulin binds primarily to site 1 and contacts a side surface of FnIII-1′ (site 2′) at the same time (conformation 1), and (*b*) the site 1–bound insulin rotates approximately 60° around the α-CT; as a result, this insulin binds at site 2′, while also contacting the α-CT of the adjacent site 1 (conformation 2).

9. THE FUNCTIONS OF INSULIN BINDING AT SITE 1

9.1. Breaking the Autoinhibited Apo State of the Insulin Receptor

The Λ-shaped IR dimer in the absence of insulin represents a stable, autoinhibited state of IR. It is, therefore, conceivable that insulin binding is required to destabilize the autoinhibited conformation of IR. Indeed, the superimposition of the L1 and α-CT′ (site 1a)–bound insulin onto the structure of apo IR reveals that the insulin at site 1a of apo IR sterically clashes with the linker between the FnIII-1′ and FnIII-2′ domains from the adjacent protomer (85) (**Figure 5*a***). Thus, insulin binding to site 1a of apo IR pushes the FnIII-2′ domain away from the L1 domain, thereby partially disrupting the protomer–protomer interactions that are responsible for the autoinhibition of IR. The relaxed apo IR dimer would allow structural rearrangement between the two

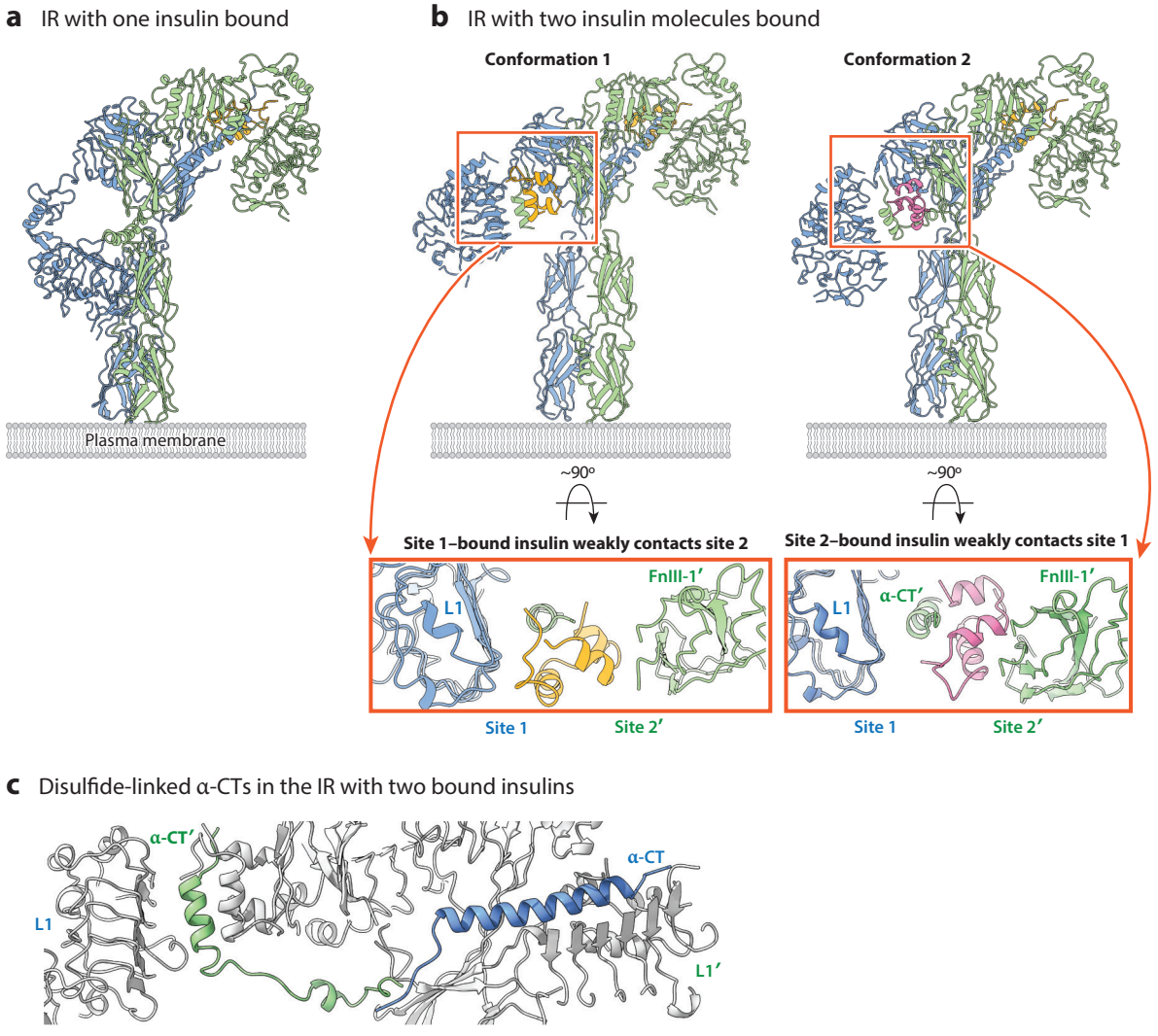

Figure 4

The cryo-EM structures of full-length IR bound with a subsaturated insulin concentration. (*a*) The cryo-EM structure of IR with a single bound insulin molecule, showing a Γ shape. (*b*) The cryo-EM structure of IR with two insulin molecules bound, showing two different types of asymmetric *T* shape. In the middle region of conformation 1, site 1–bound insulin also weakly contacts site 2. In the middle region of conformation 2, site 2–bound insulin also weakly contacts site 1. (*c*) The disulfide-linked α-CTs adopt stretched conformations in the *T*-shaped IR with two insulin molecules bound. Abbreviations: α-CT, C-terminal domain of the α subunit; cryo-EM, cryo–electron microscopy; FnIII, fibronectin type III domain; IR, insulin receptor; L, leucine-rich repeat.

protomers, leading to a T-shaped active conformation. A similar mechanism has been proposed for the IGF1-induced activation of IGF1R (95).

9.2. Stabilizing the Active State of the Insulin Receptor

The structural comparison between the Λ-shaped (apo state) and T-shaped (active state) conformations of IR indicates that, once site 1–bound insulin disrupts the autoinhibited IR, receptor activation is achieved by dramatic conformational changes that include both interprotomer

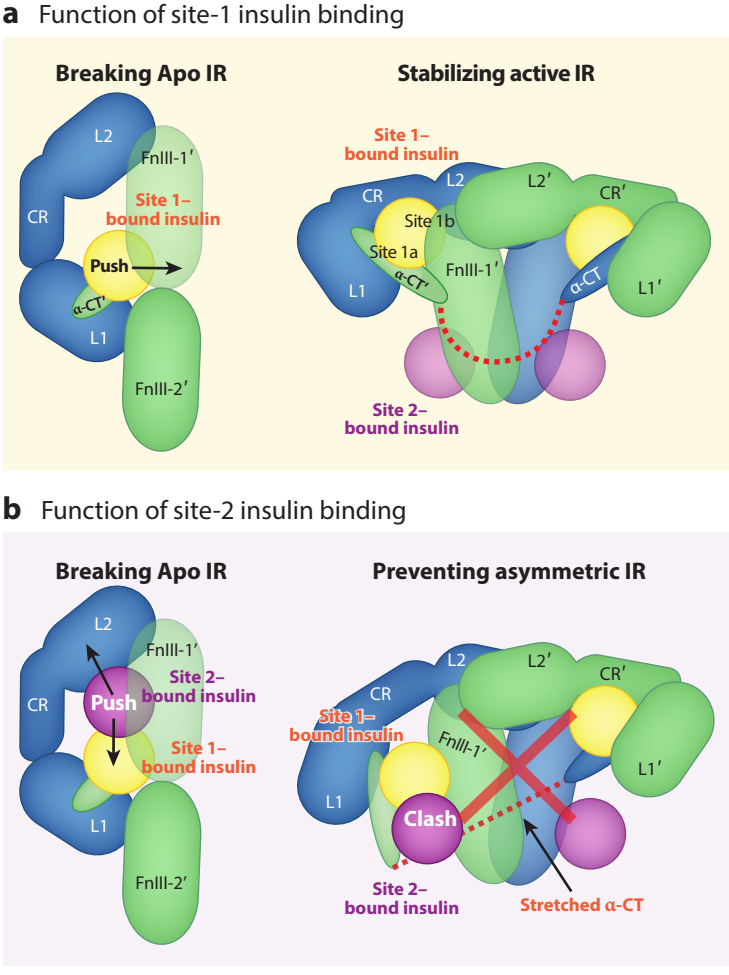

Figure 5

The functions of insulin binding at sites 1 and 2. (*a*) Site 1–bound insulin plays a critical role in insulin-induced IR activation by breaking the autoinhibited conformation of IR and by stabilizing the active conformation. (*b*) Site 2–bound insulin plays an auxiliary role in insulin-induced IR activation by assisting site 1–bound insulin in breaking the autoinhibited conformation of IR and by preventing the formation of asymmetric IR. Abbreviations: α-CT, C-terminal domain of the α subunit; cryo-EM, cryo–electron microscopy; FnIII, fibronectin type III domain; IR, insulin receptor; L, leucine-rich repeat.

rotation and an intraprotomer hinge motion. In the T-shaped active IR dimer, insulin bound at site 1 stabilizes the active conformation by simultaneously contacting several domains between the two protomers, including the L1 of one protomer, and the α-CT′ and FnIII-1′ of another (**Figure 5*a***). Thus, site 1–bound insulin tightly cross-links the two protomers in the T-shaped IR.

10. THE FUNCTION OF INSULIN BINDING AT SITE 2

10.1. Assisting Site 1–Bound Insulin in Breaking the Autoinhibited Insulin Receptor State

Insulin binding to site 1a of apo IR separates the L1 domain of one protomer from the FnIII-2′ domain of the other in the middle part of the Λ-shaped IR dimer. Nevertheless, due to the long

interdomain linkers in each protomer, the interactions between the L2 and FnIII-1′ domains in the top part of the Λ remain intact, even with insulin bound at site 1a. This suggests that site 1–bound insulins may not be able to completely disrupt the autoinhibited state of IR. The cryo-EM analysis of full-length IR with insulin bound only at site 2 demonstrates that insulin can bind to site 2 in the apo IR without changing the conformation of IR (92). In addition, the two insulin molecules bound at sites 1a and 2 in one half of the apo IR would clash (85) (**Figure 5*b***). Such a steric clash may push the site 2–bound insulin and its bound FnIII-1′ domain away from the L2 domain of the adjacent protomer, thereby further separating the two protomers (**Figure 5*b***). Thus, it is likely that the insulins bound at sites 1 and 2 cooperatively disrupt the autoinhibited state of IR.

10.2. Preventing the Formation of Asymmetric Conformations of Insulin Receptor

IR predominantly forms asymmetric conformations when two insulin molecules are bound at the IR site 1s (**Figure 4*b***), in contrast to the T-shaped symmetric conformation induced by the binding of four insulin molecules to both sites 1 and 2 (92, 93). This structural observation suggests that insulin binding to site 2 prevents the formation of asymmetric conformations of IR. In other words, insulin binding to site 2 is necessary to overcome the energetic hurdle associated with the asymmetric state of IR, allowing IR to reach a more stable, symmetric T shape.

The cryo-EM data from the full-length IR obtained at subsaturating insulin concentrations provide a structural explanation for why IR cannot form an asymmetric conformation when four insulin molecules are bound to both site 1 and 2 (92). In the middle part of the *T*-shaped asymmetric IR with two insulin molecules bound at site 1s, one insulin primarily binds to site 1 but also weakly contacts site 2′ (hybrid site) (**Figure 4*b***). The binding of another insulin to the site 2′ within the hybrid site would require an outward movement of the lower L1 and α-CT domain to prevent steric clashes between the two insulin molecules. However, the two disulfide-linked α-CTs in the *T*-shaped IR adopt a kinked and extended conformation (**Figure 4*c***). Such stretched α-CTs restrict the outward movement of the lower L1 domain, preventing the binding of another insulin to the hybrid site in the *T*-shaped IR (**Figure 5*b***). Given these structural observations, we propose that, upon the binding of four insulin molecules to both sites 1 and 2, the L1 and α-CT′ domain, together with bound insulin (i.e., site 1a), must move upward, ultimately reaching the top loop of the FnIII-1′ domain (i.e., site 1b), to prevent both (*a*) the clash with the site 2–bound insulin and (*b*) the overstretching of the two disulfide-linked α-CTs. As a result, the T-shaped symmetric dimer would be formed exclusively. Collectively, these structural results and analyses explain how the binding of insulin to site 2 prevents the formation of asymmetric IR, as well as why only the T-shaped IR has been observed in cryo-EM data sets of IR at saturating insulin concentrations (85, 92).

Furthermore, a recent study using site-specific insulin mutants supports the functional significance of insulin binding at site 2 (92) in the following ways. (*a*) Insulin mutants that bind only to IR site 2 (insulin site-1 mutants) fail to disrupt the apo IR. Conversely, insulin mutants that bind only to IR site 1 (insulin site-2 mutants) break the apo IR, but most of the IR bound to insulin site-2 mutants forms asymmetric conformations. (*b*) Insulin site-2 mutants displayed greatly reduced potency for triggering IR autophosphorylation compared with native insulin. (*c*) Neither insulin site-1 nor site-2 mutants alone reduced blood glucose levels in mice. However, cotreatment with a 1:1 stoichiometry of the insulin site-1 and site-2 mutants activated IR signaling and lowered blood glucose levels in mice. (*d*) Consistent with the functional results, the structure of IR with both insulin site-1 and site-2 mutants bound exhibits a symmetric T shape, identical to the T-shaped IR with four native insulin molecules. These structural and functional data together

suggest that insulin binding at site 2 plays a critical role in regulating the conformation of IR, i.e., converting IR from asymmetric to symmetric conformations, and clearly demonstrate that the binding of multiple insulin molecules to both site 1 and site 2 facilitates optimal IR signaling by promoting the T-shaped symmetric conformation.

11. INSULIN-DEPENDENT INSULIN RECEPTOR ACTIVATION

11.1. Proposed Activation Mechanism of the Insulin Receptor in Response to the Binding of a Single Insulin Molecule

In principle, insulin should prefer to bind to IR site 1, as site 1 has an affinity for insulin more than tenfold higher than that of site 2. The binding of one insulin to one of the two site 1s of apo IR breaks one of the two L1–FnIII-2′ interactions that are critical for the maintenance of the apo IR, thus partially disrupting the autoinhibited conformation; a similar process is observed during IGF1R activation by IGF1 (**Figure 6*a***). The released L1′ and α-CT domains (site 1a), along with bound insulin, undergo a hinge motion and move upward, making contact with the top loop of the FnIII-1 domain (site 1b) from the neighboring protomer, forming the top part of the Γ-shaped IR dimer (**Figure 6*a***). The released FnIII-1−3 domains of another protomer swing toward to the neighboring leg and make close contact with the L1 domain of the same protomer in the bottom part of the Γ (**Figure 6*a***). This swing motion of FnIII-1−3 reduces the distance between the two membrane-proximal domains, thus facilitating autophosphorylation. The L1–FnIII-2′ interaction in the unliganded half of the IR remains unchanged in comparison to the apo IR. In addition, the two covalently linked α-CTs form a rigid beam-like structure, further contributing to the structural stability of the Γ-shaped asymmetric IR with one insulin molecule bound (92).

11.2. Proposed Activation Mechanism of the Insulin Receptor in Response to the Binding of Two Insulin Molecules Only to Site 1s

IR with two insulin molecules bound at site 1s predominately assumes an asymmetric conformation (92). In this asymmetric IR, protomer I has a 7-shaped conformation almost identical to that in the Λ-shaped IR (**Figure 7*a*,*b***), while protomer II retains a similar leg to that of protomer I with a different conformation of the head part—extended versus compacted. This structural analysis hints that, after the apo IR is disrupted by the insulin binding to two site 1s, a certain degree of IR activation could be achieved by a scissor-like rotation between the two protomers as rigid bodies, using the interface between the L2 and FnIII-1′ domains as a pivot point (**Figure 6*b***). In principle, this would result in an extended T-shaped IR with membrane-proximal stalks placed in close proximity. During the structural transition, however, the two L1 domains and disulfide-linked α-CTs would be separated by a long distance. As a consequence, the two disulfide-linked α-CTs would adopt a straightened and stretched conformation (similar to the rope in a game of tug-of-war), which may be energetically unfavorable (**Figure 6*b***). This indicates that the extended T-shaped conformation must be unstable and may represent a transition state during IR activation.

We speculate that the structural instability of the extended T-shaped IR would be reduced through spontaneous hinge motions of the L1, α-CT′, CR, and L2 domains within one or both protomers, which would convert one or both protomers from an extended to a compacted conformation, leading to a *T*-shaped asymmetric or T-shaped symmetric architecture (**Figure 6*b***). Indeed, these two distinct IR conformations were observed in cryo-EM data from full-length IR obtained at subsaturating insulin concentrations (92) (**Figure 4*b***). In the *T*- or compacted T-shaped IR, the distance between the two L1 domains was reduced, allowing the disulfide-linked α-CTs to bridge them more easily. On the other hand, it is reasonable to imagine that the

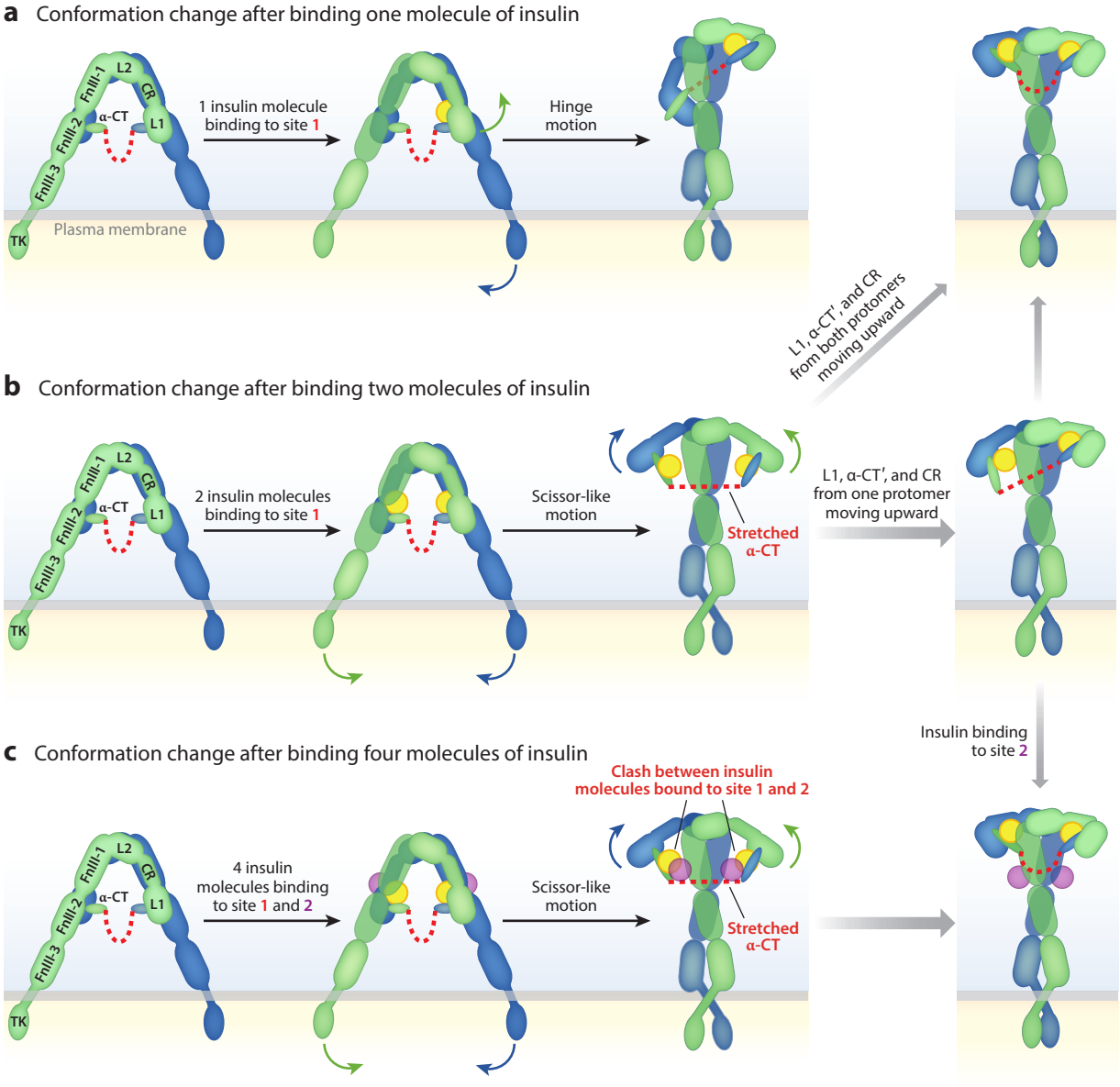

Figure 6

The proposed model of insulin-induced IR activation. At unsaturated insulin concentrations, one or two insulin molecules bind to IR site 1(s) and disrupt the autoinhibited conformation. (*a*) The released L1 and α-CT′ domains with a site 1a–bound insulin move upward to the top loop of FnIII-1′ (site 1b), cross-linking two protomers. (*b*) Two insulin molecules binding at both IR site 1s facilitate a scissor-like rotation of the two protomers. We speculate that these conformational changes lead to an unstable intermediate state of IR. We further propose that hinge motions between the L1, α-CT′, CR, and L2 domains within one or both protomers reduce the structural instability, resulting in *T*-shaped asymmetric or T-shaped symmetric IR dimers. (*c*) At saturating insulin concentrations, four insulin molecules bind to IR sites 1 and 2, breaking the autoinhibited conformation effectively and promoting a scissor-like rotation of the two protomers. The collision between two insulin molecules at sites 1 and 2 in combination with the tension generated by disulfide-linked α-CTs promotes the formation of the fully active, T-shaped IR. Abbreviations: α-CT, C-terminal domain of the α subunit; CR, cysteine-rich region; FnIII, fibronectin type III domain; IR, insulin receptor; L, leucine-rich repeat; TK, tyrosine kinase.

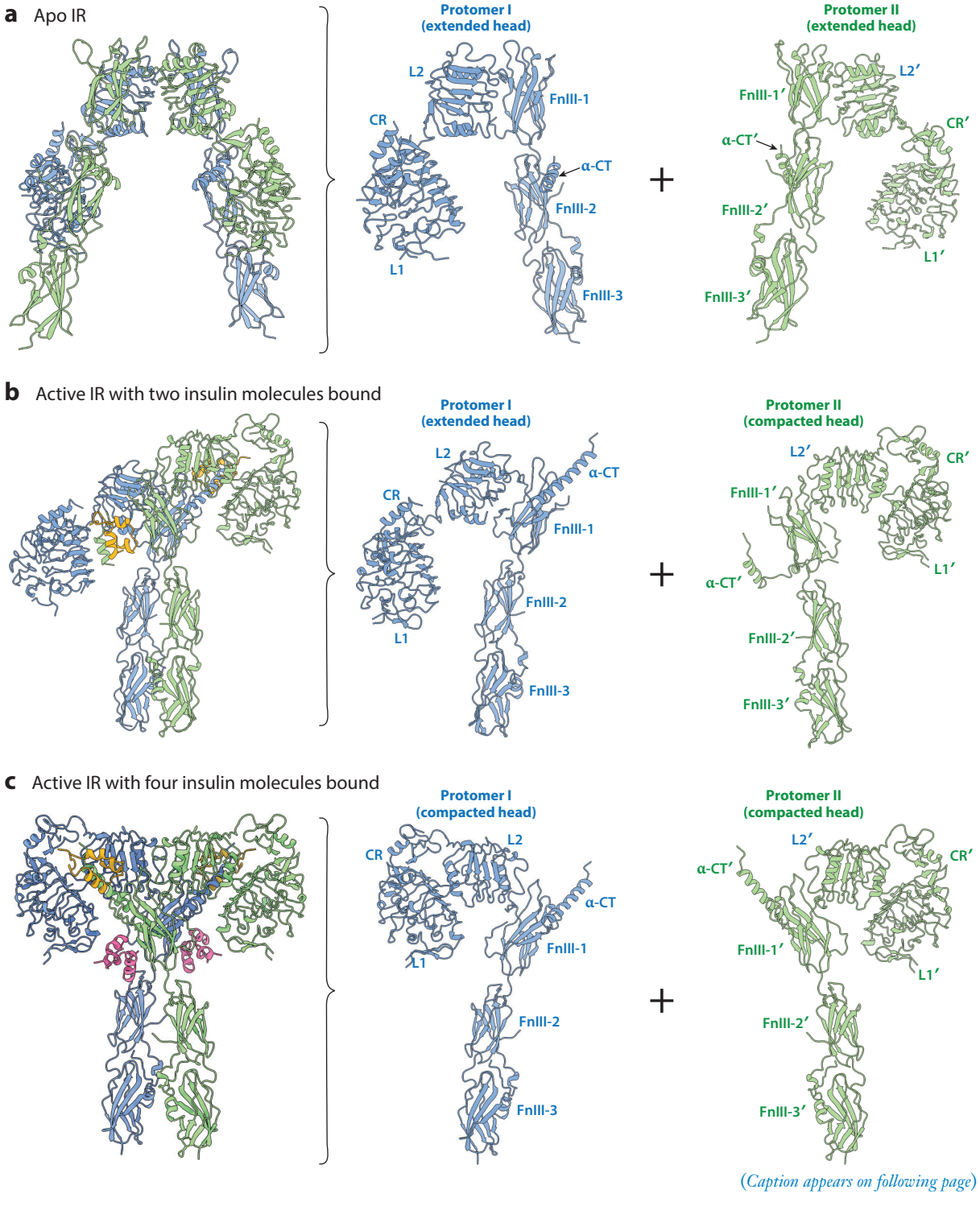

(*Caption appears on following page*)

Figure 7 (*Figure appears on preceding page*)

The protomer conformations of IR with different numbers of insulin molecules bound. Two different types of IR protomer conformations exist, compacted and extended. (*a*) The apo IR consists of two extended protomers. (*b*) The *T*-shaped IR with two insulin molecules bound consists of one extended protomer and one compacted protomer. (*c*) The T-shaped IR with four insulin molecules bound consists of two compacted protomers. Abbreviations: α-CT, C-terminal domain of the α subunit; CR, cysteine-rich region; FnIII, fibronectin type III domain; IR, insulin receptor; L, leucine-rich repeat.

straightened disulfide-linked α-CTs in the extended T-shaped IR would act as a stretched spring to generate large contraction forces that promote the conformational rearrangement of IR from the extended T-shape to a *T*- or compacted T-shape (**Figure 6*b***).

Two different types of insulin binding to site 1 in the top and middle regions of *T* stabilize the *T*-shaped asymmetric IR (**Figure 4*b***). However, the *T*-shaped IR is not likely to be very stable, as insulin bound at site 1 of one protomer in the middle part of the complex makes only weak contact with the site 2′ of another protomer. Thus, the *T*-shaped asymmetric IR may represent a local energy minimum and a partially active state. Consistently, IR exhibits lower activity in response to insulin mutants that can bind only to IR site 1 (92).

11.3. Proposed Activation Mechanism of Insulin Receptor in Response to the Binding of Four Insulin Molecules to Both Sites 1 and 2

The insulin-binding surface of site 2 in the apo IR is exposed. Furthermore, cryo-EM analysis of IR with insulin bound only at site 2 demonstrates that insulin can bind to site 2 in the apo IR without altering its overall conformation (92). It is, therefore, tempting to speculate that four insulin molecules are able to bind to all the sites (i.e., two site 1s and two site 2s) at saturating insulin concentrations (**Figure 6*c***). Four insulin molecules binding to two types of site in apo IR could more effectively disrupt the autoinhibited conformation and trigger a scissor-like rotation between two rigid protomers, leading to an extended T-shaped conformation (**Figure 6*c***). However, the extended T-shaped IR is unstable for the following reasons: (*a*) The disulfide-linked α-CTs would adopt an extended and stretched conformation, due to the long distance between the two L1 domains, and (*b*) insulin molecules bound at sites 1 and 2′ are most likely to collide with each other on both sides of the extended T, owing to the limited space between sites 1 and 2′ from two adjacent protomers, similar to that shown in the hybrid site of the *T*-shaped IR (**Figures 4*b*** and **5*b***). Therefore, both the tension generated by the overstretched, disulfide-linked α-CTs and the repulsive force generated by the collision between two insulin molecules at sites 1 and 2′ would trigger the rapid kinking movements of the L1, α-CT′, CR, and L2 domains in both protomers (**Figure 6*c***). As a result, the two L1 and α-CT′ domains (site 1a), together with their bound insulin, would move upward and ultimately touch the top surface of the FnIII-1′ domain (site 1b); consequently, the head parts of the two protomers would adopt a compacted conformation, and the IR would be transformed from an extended T to a compacted T-shaped conformation (**Figures 6*c*** and **7*c***). The T-shaped symmetric conformation was exclusively observed in the cryo-EM data set of full-length IR obtained at a saturating insulin concentration, supporting this activation model. Moreover, recent cryo-EM studies demonstrate that IR with physically decoupled α-CT predominantly adopts asymmetric conformations even at saturating insulin concentrations (96). This finding further supports the proposed activation model that both disulfide-linked α-CTs and insulin binding at two distinct sites are critical for the efficient formation of the fully active, T-shaped IR.

The T-shaped IR dimer is structurally stable due to the concurrent binding of insulin to both sites 1a and 1b, as well as extensive protomer–protomer interactions. In addition, the disulfide-linked α-CTs in this compacted T-shape assume a relaxed conformation due to the short distance

between their two L1 domains. Collectively, these structural observations suggest that the T-shaped symmetric IR conformation has the highest structural stability and may represent the most optimal state for IR activation.

12. SOURCES OF NEGATIVE COOPERATIVITY

Insulin binds to IR with a complex kinetics characterized by a curvilinear Scatchard plot, suggesting a negative cooperativity in the binding of insulin to IR (35). Recent cryo-EM studies of the full-length IR bound to different numbers of insulin molecules provide a structural basis for understanding the source of negative cooperativity (92).

Structural plasticity of α-CT in IR is required for insulin binding. In the apo IR, only the N-terminal part of α-CT is folded as a short α-helix, whereas the rest of this motif is disordered (76). This partially folded α-CT without any constraints in both the N and C termini can undergo the conformational change that is necessary for insulin binding. In the Γ-shaped IR dimer (with only one insulin molecule bound at site 1), the disulfide-linked α-CTs adopt a rigid and elongated conformation (92) (**Figure 4*a***). In this structural configuration, the conformational plasticity of the unliganded α-CT is restricted. Thus, the unliganded α-CT in the asymmetric IR dimer is likely to be less capable of binding insulin, suggesting a negative cooperativity between the two site 1s. A similar molecular mechanism underlying the negative cooperativity in the binding of IGF1 to IGF1R has been proposed before (94). Furthermore, in the middle region of the *T*-shaped IR (with two insulin molecules bound), sites 1 and 2′ from two neighbor protomers are located in close proximity and largely overlap (**Figure 4*b***). Therefore, the binding of insulin at site 1 hinders the binding of another insulin to site 2′, or vice versa, thereby underlying the potential negative cooperativity between sites 1 and 2′ in the *T*-shaped IR.

13. THE FUNCTIONAL IMPORTANCE OF α-CT

The cryo-EM structure of insulin-bound full-length IR-3CS (which has the cysteine triplets in α-CT substituted with serine, i.e., C682S, C683S, C685S) demonstrated that the IR with noncovalently linked α-CTs forms predominantly asymmetric conformations, despite insulin molecules occupying all four binding sites (96). In half of these asymmetric conformations, insulin binds at site 1 and site 2′, similar to the T-shaped IR, while in the other half, two insulin molecules bind to the hybrid site without stretching the α-CTs. The fact that fully liganded IR with physically decoupled α-CTs adopts asymmetric conformations supports the idea that disulfide-linked α-CTs play a critical role in promoting the T-shaped symmetric IR. In addition, the levels of phosphorylation of AKT and ERK were markedly reduced in cells expressing IR-3CS, further suggesting that disulfide linkages between two α-CTs are essential for the formation of the T-shaped IR dimer and optimal IR function (96).

14. COMPARING THE ACTIVATION MECHANISMS OF THE INSULIN RECEPTOR AND THE INSULIN-LIKE GROWTH FACTOR 1 RECEPTOR

Despite the fact that IR and IGF1R share high levels of structural similarity, ligand binding differs between these two receptors (97). Recent cryo-EM studies have demonstrated that the activation mechanism of IR differs significantly from that of the IGF1R. In contrast to the maximum 2:4 stoichiometry of the active IR–insulin complex, IGF1 is undetectable in the side surface of FnIII-1 in IGF1R (equivalent to site 2 of IR), and a single IGF1 bound to IGF1R is sufficient to fully activate the receptor (94).

Additionally, in the fully liganded, active state of IR, the stalks of the dimer that contain the FnIII-2 and FnIII-3 domains are closely associated by homotypic interactions between two loops in the FnIII-2 domain (85). In the fully active state of IGF1R, however, the unliganded L1 domain bridges the two stalks of the dimer into close proximity and further stabilizes the active conformation (94). It is possible that the different arrangements of the membrane-proximal stalk regions between IR and IGF1R may provide a mechanism for defining their signaling specificity, allowing these two closely related receptors to generate distinct signaling outcomes.

Notably, to facilitate timely metabolic activity, the circulating levels of insulin rapidly fluctuate in response to food intake and exercise. In contrast, IGF1 levels remain unchanged during the daytime and are responsible for long-term actions such as cell growth and differentiation (98–100). As IR has different insulin-binding occupancy under different blood insulin concentrations, such a unique multisite system allows IR to respond to a wide range of insulin concentrations in different metabolic states. In contrast, the one-site system in IGF1R allows it to respond to IGF1 binding with high sensitivity. In part, this explains why these two related receptors use remarkably different mechanisms for activation.

15. NEGATIVE REGULATORS OF INSULIN RECEPTOR SIGNALING

As insulin has multiple functions and is crucial to systemic homeostasis, IR signaling should be tightly fine-tuned. Insulin itself contributes to the termination of IR signaling by promoting IR endocytosis, and groups of phosphatases suppress the action of insulin in multiple steps. In addition, the levels of IR on the cell surface are regulated by ubiquitin-mediated degradation. These mechanisms are largely redundant and vary depending on the tissue, developmental stage, and health condition.

15.1. Insulin Receptor Endocytosis

Insulin-activated IR undergoes clathrin- or caveolae-mediated endocytosis, which controls spatiotemporal IR signaling, insulin clearance, and insulin delivery (25, 74, 101–104). The IR autophosphorylation and downstream signaling proteins control the clathrin-mediated IR endocytosis, which allows activated IR to be preferentially internalized (38, 87, 105–107). The internalized IR undergoes lysosomal degradation or recycles back to the plasma membrane. Thus, persistent hyperinsulinemia, which is closely related to insulin resistance, promotes IR endocytosis, and inhibits IR signaling. Consistent with this idea, IR levels on the cell surface are reduced in the livers of type 2 diabetes patients (108, 109) and insulin resistant mice (110). Assembly polypeptide 2 (AP2) links IR to clathrin, thus promoting IR endocytosis. The SHP2–MAPK axis controls the phosphorylation of IRS, thus facilitating the association of IRS–AP2 with IR (74, 108). In addition, the cell division regulators mitotic arrest deficient 2 (MAD2), budding uninhibited by benzimidazole-related 1 (BUBR1), cell division cycle protein 20 homolog (CDC20), and $p31^{comet}$ directly control the association of AP2 with IR, thus regulating IR endocytosis (87, 102).

15.2. Ubiquitination

Several E3 ubiquitin ligases negatively regulate IR signaling by targeting IR and IRS. The canonical model of IR ubiquitination is that E3 ubiquitin protein ligases (e.g., NEDD4 and CBL) ubiquitinate IR, facilitating IR endocytosis and endosomal trafficking, thereby downregulating IR signaling (101). In addition to the canonical model, SOCS family proteins also inhibit IR signaling by recruiting E3 ubiquitin ligases to IR or IRS and promoting proteasomal degradation (111). Moreover, Mitsugumin 53 (MG53) has been proposed to ubiquitinate IR and IRS1 in

skeletal muscle (112, 113). Recently, RNAi screening identified MARCH1 as an E3 ligase of IR, demonstrating that MARCH1 regulates basal levels of IR in liver (114).

15.3. Phosphatases

Two types of phosphatases terminate IR signaling: lipid and protein phosphatases. PTEN and SH2-containing inositol 5′-phosphatase 2 (SHIP2) dephosphorylate the lipid second messenger phosphatidylinositol 3,4,5-triphosphate [$PI(3,4,5)P_3$], thereby attenuating IR signaling (**Figure 1*b***). PTEN converts $PI(3,4,5)P_3$ to $PI(4,5)P_2$, whereas SHIP2 converts $PI(3,4,5)P_3$ to $PI(3,4)P_2$, terminating PI3K signaling (115–117). In addition, protein-tyrosine phosphatase 1B (PTP1B) is a well-characterized tyrosine phosphatase localized at the endoplasmic reticulum that negatively regulates IR signaling through direct binding to IR (118–120).

16. INSULIN RECEPTOR AND INSULIN-LIKE GROWTH FACTOR 1 RECEPTOR HYBRIDS

Previous studies have demonstrated that a hybrid receptor may be composed of one protomer from IR and the other from IGF1R, thus forming a heterotetramer (121, 122). A combined binding assay with labeled IGF1 and monoclonal antibodies specific to IR or IGF1R demonstrated that these hybrid receptors could bind both insulin and IGF1 with high binding affinity, showing potential functional properties (123). It has been proposed that there is variation in the expression levels of the IR–IGF1R hybrid in different tissues, and the IR–IGF1R hybrid is the major form of IGF1R in muscle (124). The two isoforms of IR can form hybrid receptors with IGF1R with similar efficiency; however, IR-A–IGF1R and IR-B–IGF1R hybrid receptors have different ligand-binding affinities and activation potencies in response to insulin and IGF2 (125). The IR-A–IGF1R hybrid binds to IGF2 with high affinity compared with IR-B–IGF1R.

Given the distinct activation mechanisms of IR and IGF1R, the mechanism for ligand binding and activation of the hybrid receptor is likely to be complicated. Moreover, the factors and mechanisms that regulate the formation of IR–IGF1R hybrids, as well as the physiological functions of the hybrid receptors, are unknown. The recent structure of the IGF1-bound ECD of an IR-B–IGF1R hybrid receptor demonstrates that IGF1 binds to the L1 and CR domains of IGF1R and the FnIII-1 domain of IR (126). The overall structure of the IGF1-bound IR-B–IGF1R hybrid receptor resembled the asymmetric conformation shown in IGF1R–IGF1 (94), IGF1Rzip–IGF2 (zipper stabilized IGF1R ECD) (127), IGF1R–insulin (128), and IRzip–insulin (zipper stabilized IR ECD) (81). Future studies are required to determine the structure of the apo IR–IGF1R as well as the full-length structures of the IR–IGF1R hybrid with different ligands bound.

17. CONCLUSIONS AND PERSPECTIVES

The recent advances in structural and functional studies of IR have significantly contributed to our understanding of IR activation. In addition to long-term studies of this important receptor using biochemistry and X-ray crystallography, recent developments in single-particle cryo-EM have allowed high-resolution structural determinations of the dynamic IR–insulin complex (129). It is clear, however, that more remains to be learned about the activation mechanism of IR and its downstream signaling.

The TM domains in IR are critical for receptor activation and downstream signaling (130, 131). Visualizing the TMs in their dimerized active form and revealing the dimerization interface are important steps toward fully understanding the activation mechanism of IR. Additionally, because the FnIII-3 domain is connected to the TM domain through a short linker (4 residues),

it is reasonable to speculate that the ECD, TM domain, and ICD are coupled allosterically and that differences in the arrangements of the membrane-proximal regions in the asymmetric and symmetric IR may cause differential dimeric assembly of the TM domain and ICD. However, as of now, no cryo-EM structures of full-length IR–insulin complexes have been able to resolve a complete structure of IR, due to the flexible linkages of the TM helix with both the ECD and ICD. It may be necessary to stabilize the junction at the two ends of the TM domains using accessory factors such as conformationally selective nanobodies and TM-associating peptides (132). The cryo-EM density of the TM domains could also be improved by the application of advanced focused image classification techniques to distinguish different conformational states of the TM of IR (133). In addition, the reconstitution of full-length IR into a lipid bilayer, such as a nanodisc, saposin lipid nanoparticle, or peptidisc (134–136), may stabilize the TM domains by lipid–TM interaction and further improve the resolution. Certain types of lipids, such as phosphatidylinositol, have been suggested to play a key role in stabilizing the ICD of a variety of RTKs (137), including IR. Therefore, integrating such lipids into the nanodisc during sample preparation may facilitate determining the entire structure of the full-length IR–insulin complex.

Furthermore, IR has a large number of protein partners that play critical roles in promoting and regulating IR signaling (138). It remains challenging to determine the structure of full-length IR bound to downstream signaling proteins or other binding partners for the following reasons: (*a*) Those binding partners are associated with IR transiently; (*b*) the binding of most signaling proteins to IR requires receptor phosphorylation; and (*c*) the relative orientation between IR and its binding partners may not be fixed. It is important to note that all of the previously purified full-length IRs used for structural studies are kinase dead and cannot undergo autophosphorylation. In addition, a key IRS-binding region of IR (the NPEY960 motif) was mutated to prevent IR endocytosis. Thus, it would be essential to purify the overexpressed full-length wild-type IR or directly isolate IR from a native source to reconstitute IR–insulin in complex with their binding partners in vitro. Subsequently, the combination of biochemistry, mass spectrometry, X-ray crystallography, single-particle cryo-EM, cryo-electron tomography (139), and computational modelling [e.g., Alpha fold (140)] will make it possible to visualize the entire structure of the IR signaling complex, thus providing a comprehensive understanding of the mechanism of IR signaling. A complete understanding of the structural nature of IR and the IR signaling complex will assist in the development of novel therapeutics for diseases associated with dysregulation of IR signaling.

DISCLOSURE STATEMENT

The authors are not aware of any affiliations, memberships, funding, or financial holdings that might be perceived as affecting the objectivity of this review.

ACKNOWLEDGMENTS

This work is supported in part by grants from the National Institutes Health (R01GM136976 to X.-C.B. and R01DK132361 to E.C.), the Welch foundation (I-1944 to X.-C.B.), and the Alice Bohmfalk Charitable Trust (to E.C.). X.-C.B. is a Virginia Murchison Linthicum Scholar in Medical Research at the University of Texas Southwestern Medical Center.

LITERATURE CITED

1. Banting FG, Best CH, Collip JB, Campbell WR, Fletcher AA. 1922. Pancreatic extracts in the treatment of diabetes mellitus. *Can. Med. Assoc. J.* 12:141–46

2. Levine R, Goldstein MS, Huddlestun B, Klein SP. 1950. Action of insulin on the 'permeability' of cells to free hexoses, as studied by its effect on the distribution of galactose. *Am. J. Physiol.* 163:70–76
3. Freychet P, Roth J, Neville DM Jr. 1971. Insulin receptors in the liver: specific binding of [^{125}I]insulin to the plasma membrane and its relation to insulin bioactivity. *PNAS* 68:1833–37
4. Kasuga M, Karlsson FA, Kahn CR. 1982. Insulin stimulates the phosphorylation of the 95,000-dalton subunit of its own receptor. *Science* 215:185–87
5. Kasuga M, Zick Y, Blithe DL, Crettaz M, Kahn CR. 1982. Insulin stimulates tyrosine phosphorylation of the insulin receptor in a cell-free system. *Nature* 298:667–69
6. Ullrich A, Bell JR, Chen EY, Herrera R, Petruzzelli LM, et al. 1985. Human insulin receptor and its relationship to the tyrosine kinase family of oncogenes. *Nature* 313:756–61
7. Ebina Y, Ellis L, Jarnagin K, Edery M, Graf L, et al. 1985. The human insulin receptor cDNA: the structural basis for hormone-activated transmembrane signalling. *Cell* 40:747–58
8. Ullrich A, Gray A, Tam AW, Yang-Feng T, Tsubokawa M, et al. 1986. Insulin-like growth factor I receptor primary structure: comparison with insulin receptor suggests structural determinants that define functional specificity. *EMBO J.* 5:2503–12
9. Shier P, Watt VM. 1989. Primary structure of a putative receptor for a ligand of the insulin family. *J. Biol. Chem.* 264:14605–8
10. Bravo DA, Gleason JB, Sanchez RI, Roth RA, Fuller RS. 1994. Accurate and efficient cleavage of the human insulin proreceptor by the human proprotein-processing protease furin. Characterization and kinetic parameters using the purified, secreted soluble protease expressed by a recombinant baculovirus. *J. Biol. Chem.* 269:25830–37
11. Bajaj M, Waterfield MD, Schlessinger J, Taylor WR, Blundell T. 1987. On the tertiary structure of the extracellular domains of the epidermal growth factor and insulin receptors. *Biochim. Biophys. Acta* 916:220–26
12. Schaffer L, Ljungqvist L. 1992. Identification of a disulfide bridge connecting the α-subunits of the extracellular domain of the insulin receptor. *Biochem. Biophys. Res. Commun.* 189:650–53
13. Sparrow LG, McKern NM, Gorman JJ, Strike PM, Robinson CP, et al. 1997. The disulfide bonds in the C-terminal domains of the human insulin receptor ectodomain. *J. Biol. Chem.* 272:29460–67
14. Seino S, Bell GI. 1989. Alternative splicing of human insulin receptor messenger RNA. *Biochem. Biophys. Res. Commun.* 159:312–16
15. Frasca F, Pandini G, Scalia P, Sciacca L, Mineo R, et al. 1999. Insulin receptor isoform A, a newly recognized, high-affinity insulin-like growth factor II receptor in fetal and cancer cells. *Mol. Cell. Biol.* 19:3278–88
16. Petersen MC, Shulman GI. 2018. Mechanisms of insulin action and insulin resistance. *Physiol. Rev.* 98:2133–223
17. Santoro A, McGraw TE, Kahn BB. 2021. Insulin action in adipocytes, adipose remodeling, and systemic effects. *Cell Metab.* 33:748–57
18. Rask-Madsen C, Kahn CR. 2012. Tissue-specific insulin signaling, metabolic syndrome, and cardiovascular disease. *Arterioscler Thromb. Vasc. Biol.* 32:2052–59
19. Nandi A, Kitamura Y, Kahn CR, Accili D. 2004. Mouse models of insulin resistance. *Physiol. Rev.* 84:623–47
20. Samuel VT, Shulman GI. 2016. The pathogenesis of insulin resistance: integrating signaling pathways and substrate flux. *J. Clin. Investig.* 126:12–22
21. Kullmann S, Heni M, Hallschmid M, Fritsche A, Preissl H, Haring HU. 2016. Brain insulin resistance at the crossroads of metabolic and cognitive disorders in humans. *Physiol. Rev.* 96:1169–209
22. Arnold SE, Arvanitakis Z, Macauley-Rambach SL, Koenig AM, Wang HY, et al. 2018. Brain insulin resistance in type 2 diabetes and Alzheimer disease: concepts and conundrums. *Nat. Rev. Neurol.* 14:168–81
23. Tsai S, Clemente-Casares X, Zhou AC, Lei H, Ahn JJ, et al. 2018. Insulin receptor-mediated stimulation boosts T cell immunity during inflammation and infection. *Cell Metab.* 28:922–34.e4
24. Pulgar VM. 2018. Transcytosis to cross the blood brain barrier, new advancements and challenges. *Front. Neurosci.* 12:1019

25. Lee WL, Klip A. 2016. Endothelial transcytosis of insulin: Does it contribute to insulin resistance? *Physiology* 31:336–45
26. Hubbard SR, Wei L, Ellis L, Hendrickson WA. 1994. Crystal structure of the tyrosine kinase domain of the human insulin receptor. *Nature* 372:746–54
27. Eck MJ, Dhe-Paganon S, Trub T, Nolte RT, Shoelson SE. 1996. Structure of the IRS-1 PTB domain bound to the juxtamembrane region of the insulin receptor. *Cell* 85:695–705
28. Salmeen A, Andersen JN, Myers MP, Tonks NK, Barford D. 2000. Molecular basis for the dephosphorylation of the activation segment of the insulin receptor by protein tyrosine phosphatase 1B. *Mol. Cell* 6:1401–12
29. Hu J, Liu J, Ghirlando R, Saltiel AR, Hubbard SR. 2003. Structural basis for recruitment of the adaptor protein APS to the activated insulin receptor. *Mol. Cell* 12:1379–89
30. Depetris RS, Hu J, Gimpelevich I, Holt LJ, Daly RJ, Hubbard SR. 2005. Structural basis for inhibition of the insulin receptor by the adaptor protein Grb14. *Mol. Cell* 20:325–33
31. Haeusler RA, McGraw TE, Accili D. 2018. Biochemical and cellular properties of insulin receptor signalling. *Nat. Rev. Mol. Cell Biol.* 19:31–44
32. Boucher J, Kleinridders A, Kahn CR. 2014. Insulin receptor signaling in normal and insulin-resistant states. *Cold Spring Harb. Perspect. Biol.* 6:a009191
33. White MF, Kahn CR. 2021. Insulin action at a molecular level – 100 years of progress. *Mol. Metab.* 52:101304
34. Gavin JR 3rd, Gorden P, Roth J, Archer JA, Buell DN. 1973. Characteristics of the human lymphocyte insulin receptor. *J. Biol. Chem.* 248:2202–7
35. De Meyts P, Roth J, Neville DM Jr., Gavin JR 3rd, Lesniak MA. 1973. Insulin interactions with its receptors: experimental evidence for negative cooperativity. *Biochem. Biophys. Res. Commun.* 55:154–61
36. De Meyts P, Bainco AR, Roth J. 1976. Site-site interactions among insulin receptors. Characterization of the negative cooperativity. *J. Biol. Chem.* 251:1877–88
37. White MF, Shoelson SE, Keutmann H, Kahn CR. 1988. A cascade of tyrosine autophosphorylation in the β-subunit activates the phosphotransferase of the insulin receptor. *J. Biol. Chem.* 263:2969–80
38. Rajagopalan M, Neidigh JL, McClain DA. 1991. Amino acid sequences Gly-Pro-Leu-Tyr and Asn-Pro-Glu-Tyr in the submembranous domain of the insulin receptor are required for normal endocytosis. *J. Biol. Chem.* 266:23068–73
39. Kahn CR, White MF. 1988. The insulin receptor and the molecular mechanism of insulin action. *J. Clin. Investig.* 82:1151–56
40. Sun XJ, Rothenberg P, Kahn CR, Backer JM, Araki E, et al. 1991. Structure of the insulin receptor substrate IRS-1 defines a unique signal transduction protein. *Nature* 352:73–77
41. White MF, Maron R, Kahn CR. 1985. Insulin rapidly stimulates tyrosine phosphorylation of a M_r-185,000 protein in intact cells. *Nature* 318:183–86
42. Bjornholm M, He AR, Attersand A, Lake S, Liu SC, et al. 2002. Absence of functional insulin receptor substrate-3 (IRS-3) gene in humans. *Diabetologia* 45:1697–702
43. Sadagurski M, Dong XC, Myers MG Jr., White MF. 2014. Irs2 and Irs4 synergize in non-LepRb neurons to control energy balance and glucose homeostasis. *Mol. Metab.* 3:55–63
44. White MF, Livingston JN, Backer JM, Lauris V, Dull TJ, et al. 1988. Mutation of the insulin receptor at tyrosine 960 inhibits signal transmission but does not affect its tyrosine kinase activity. *Cell* 54:641–49
45. Backer JM, Myers MG Jr., Shoelson SE, Chin DJ, Sun XJ, et al. 1992. Phosphatidylinositol 3′-kinase is activated by association with IRS-1 during insulin stimulation. *EMBO J.* 11:3469–79
46. Kohn AD, Kovacina KS, Roth RA. 1995. Insulin stimulates the kinase activity of RAC-PK, a pleckstrin homology domain containing ser/thr kinase. *EMBO J.* 14:4288–95
47. Cantley LC. 2002. The phosphoinositide 3-kinase pathway. *Science* 296:1655–57
48. Vanhaesebroeck B, Stephens L, Hawkins P. 2012. PI3K signalling: the path to discovery and understanding. *Nat. Rev. Mol. Cell Biol.* 13:195–203
49. Cheatham B, Vlahos CJ, Cheatham L, Wang L, Blenis J, Kahn CR. 1994. Phosphatidylinositol 3-kinase activation is required for insulin stimulation of pp70 S6 kinase, DNA synthesis, and glucose transporter translocation. *Mol. Cell. Biol.* 14:4902–11

50. Hopkins BD, Pauli C, Du X, Wang DG, Li X, et al. 2018. Suppression of insulin feedback enhances the efficacy of PI3K inhibitors. *Nature* 560:499–503
51. Lu M, Wan M, Leavens KF, Chu Q, Monks BR, et al. 2012. Insulin regulates liver metabolism in vivo in the absence of hepatic Akt and Foxo1. *Nat. Med.* 18:388–95
52. Manning BD, Toker A. 2017. AKT/PKB Signaling: navigating the network. *Cell* 169:381–405
53. Suzuki K, Kono T. 1980. Evidence that insulin causes translocation of glucose transport activity to the plasma membrane from an intracellular storage site. *PNAS* 77:2542–45
54. Foley K, Boguslavsky S, Klip A. 2011. Endocytosis, recycling, and regulated exocytosis of glucose transporter 4. *Biochemistry* 50:3048–61
55. Huang S, Czech MP. 2007. The GLUT4 glucose transporter. *Cell Metab.* 5:237–52
56. Leto D, Saltiel AR. 2012. Regulation of glucose transport by insulin: traffic control of GLUT4. *Nat. Rev. Mol. Cell Biol.* 13:383–96
57. Cohen P. 1999. The Croonian Lecture 1998. Identification of a protein kinase cascade of major importance in insulin signal transduction. *Philos. Trans. R. Soc. B* 354:485–95
58. Cross DA, Alessi DR, Cohen P, Andjelkovich M, Hemmings BA. 1995. Inhibition of glycogen synthase kinase-3 by insulin mediated by protein kinase B. *Nature* 378:785–89
59. Li S, Brown MS, Goldstein JL. 2010. Bifurcation of insulin signaling pathway in rat liver: mTORC1 required for stimulation of lipogenesis, but not inhibition of gluconeogenesis. *PNAS* 107:3441–46
60. Peterson TR, Sengupta SS, Harris TE, Carmack AE, Kang SA, et al. 2011. mTOR complex 1 regulates lipin 1 localization to control the SREBP pathway. *Cell* 146:408–20
61. Laplante M, Sabatini DM. 2012. mTOR signaling in growth control and disease. *Cell* 149:274–93
62. Lin HV, Accili D. 2011. Hormonal regulation of hepatic glucose production in health and disease. *Cell Metab.* 14:9–19
63. Matsumoto M, Pocai A, Rossetti L, Depinho RA, Accili D. 2007. Impaired regulation of hepatic glucose production in mice lacking the forkhead transcription factor Foxo1 in liver. *Cell Metab.* 6:208–16
64. Nakae J, Kitamura T, Silver DL, Accili D. 2001. The forkhead transcription factor Foxo1 (Fkhr) confers insulin sensitivity onto glucose-6-phosphatase expression. *J. Clin. Investig.* 108:1359–67
65. Haeusler RA, Hartil K, Vaitheesvaran B, Arrieta-Cruz I, Knight CM, et al. 2014. Integrated control of hepatic lipogenesis versus glucose production requires FoxO transcription factors. *Nat. Commun.* 5:5190
66. Nakae J, Park BC, Accili D. 1999. Insulin stimulates phosphorylation of the forkhead transcription factor FKHR on serine 253 through a Wortmannin-sensitive pathway. *J. Biol. Chem.* 274:15982–85
67. Biggs WH 3rd, Meisenhelder J, Hunter T, Cavenee WK, Arden KC. 1999. Protein kinase B/Akt-mediated phosphorylation promotes nuclear exclusion of the winged helix transcription factor FKHR1. *PNAS* 96:7421–26
68. Gehart H, Kumpf S, Ittner A, Ricci R. 2010. MAPK signalling in cellular metabolism: stress or wellness? *EMBO Rep.* 11:834–40
69. Pronk GJ, McGlade J, Pelicci G, Pawson T, Bos JL. 1993. Insulin-induced phosphorylation of the 46- and 52-kDa Shc proteins. *J. Biol. Chem.* 268:5748–53
70. English J, Pearson G, Wilsbacher J, Swantek J, Karandikar M, et al. 1999. New insights into the control of MAP kinase pathways. *Exp. Cell Res.* 253:255–70
71. Cobb MH. 1999. MAP kinase pathways. *Prog. Biophys. Mol. Biol.* 71:479–500
72. Chen YN, LaMarche MJ, Chan HM, Fekkes P, Garcia-Fortanet J, et al. 2016. Allosteric inhibition of SHP2 phosphatase inhibits cancers driven by receptor tyrosine kinases. *Nature* 535:148–52
73. Nichols RJ, Haderk F, Stahlhut C, Schulze CJ, Hemmati G, et al. 2018. RAS nucleotide cycling underlies the SHP2 phosphatase dependence of mutant BRAF-, NF1- and RAS-driven cancers. *Nat. Cell Biol.* 20:1064–73
74. Hall C, Yu H, Choi E. 2020. Insulin receptor endocytosis in the pathophysiology of insulin resistance. *Exp. Mol. Med.* 52:911–20
75. McKern NM, Lawrence MC, Streltsov VA, Lou MZ, Adams TE, et al. 2006. Structure of the insulin receptor ectodomain reveals a folded-over conformation. *Nature* 443:218–21
76. Croll TI, Smith BJ, Margetts MB, Whittaker J, Weiss MA, et al. 2016. Higher-resolution structure of the human insulin receptor ectodomain: multi-modal inclusion of the insert domain. *Structure* 24:469–76

77. Menting JG, Whittaker J, Margetts MB, Whittaker LJ, Kong GK, et al. 2013. How insulin engages its primary binding site on the insulin receptor. *Nature* 493:241–45
78. Bai XC, McMullan G, Scheres SH. 2015. How cryo-EM is revolutionizing structural biology. *Trends Biochem. Sci.* 40:49–57
79. Cai K, Zhang X, Bai XC. 2022. Cryo-electron microscopic analysis of single-pass transmembrane receptors. *Chem. Rev.* 122:13952–88
80. Scapin G, Dandey VP, Zhang Z, Prosise W, Hruza A, et al. 2018. Structure of the insulin receptor–insulin complex by single-particle cryo-EM analysis. *Nature* 556:122–25
81. Weis F, Menting JG, Margetts MB, Chan SJ, Xu Y, et al. 2018. The signalling conformation of the insulin receptor ectodomain. *Nat. Commun.* 9:4420
82. Schaffer L. 1994. A model for insulin binding to the insulin receptor. *Eur. J. Biochem.* 221:1127–32
83. De Meyts P, Whittaker J. 2002. Structural biology of insulin and IGF1 receptors: implications for drug design. *Nat. Rev. Drug Discov.* 1:769–83
84. Whittaker J, Garcia P, Yu GQ, Mynarcik DC. 1994. Transmembrane domain interactions are necessary for negative cooperativity of the insulin receptor. *Mol. Endocrinol.* 8:1521–27
85. Uchikawa E, Choi E, Shang G, Yu H, Bai XC. 2019. Activation mechanism of the insulin receptor revealed by cryo-EM structure of the fully liganded receptor–ligand complex. *eLife* 8:e48630
86. Gutmann T, Schafer IB, Poojari C, Brankatschk B, Vattulainen I, et al. 2020. Cryo-EM structure of the complete and ligand-saturated insulin receptor ectodomain. *J. Cell Biol.* 219:e201907210
87. Choi E, Zhang X, Xing C, Yu H. 2016. Mitotic checkpoint regulators control insulin signaling and metabolic homeostasis. *Cell* 166:567–81
88. Lu D, Shang G, Zhang H, Yu Q, Cong X, et al. 2014. Structural insights into the T6SS effector protein Tse3 and the Tse3–Tsi3 complex from *Pseudomonas aeruginosa* reveal a calcium-dependent membrane-binding mechanism. *Mol. Microbiol.* 92:1092–112
89. De Meyts P. 2015. Insulin/receptor binding: the last piece of the puzzle? What recent progress on the structure of the insulin/receptor complex tells us (or not) about negative cooperativity and activation. *Bioessays* 37:389–97
90. Lawrence MC. 2021. Understanding insulin and its receptor from their three-dimensional structures. *Mol. Metab.* 52:101255
91. Kristensen C, Kjeldsen T, Wiberg FC, Schaffer L, Hach M, et al. 1997. Alanine scanning mutagenesis of insulin. *J. Biol. Chem.* 272:12978–83
92. Li J, Park J, Mayer JP, Webb KJ, Uchikawa E, et al. 2022. Synergistic activation of the insulin receptor via two distinct sites. *Nat. Struct. Mol. Biol.* 29:357–68
93. Nielsen J, Brandt J, Boesen T, Hummelshoj T, Slaaby R, et al. 2022. Structural investigations of full-length insulin receptor dynamics and signalling. *J. Mol. Biol.* 434:167458
94. Li J, Choi E, Yu H, Bai XC. 2019. Structural basis of the activation of type 1 insulin-like growth factor receptor. *Nat. Commun.* 10:4567
95. Kavran JM, McCabe JM, Byrne PO, Connacher MK, Wang Z, et al. 2014. How IGF-1 activates its receptor. *eLife* 3:e03772
96. Li J, Wu J, Hall C, Bai X-C, Choi E. 2022. Molecular basis for the role of disulfide-linked αCTs in the activation of insulin-like growth factor 1 receptor and insulin receptor. *eLife* 11:e81286
97. Nakae J, Kido Y, Accili D. 2001. Distinct and overlapping functions of insulin and IGF-I receptors. *Endocr. Rev.* 22:818–35
98. Tengholm A, Gylfe E. 2009. Oscillatory control of insulin secretion. *Mol. Cell Endocrinol.* 297:58–72
99. Siddle K. 2012. Molecular basis of signaling specificity of insulin and IGF receptors: neglected corners and recent advances. *Front. Endocrinol.* 3:34
100. Kim JJ, Accili D. 2002. Signalling through IGF-I and insulin receptors: Where is the specificity? *Growth Horm. IGF Res.* 12:84–90
101. Goh LK, Sorkin A. 2013. Endocytosis of receptor tyrosine kinases. *Cold Spring Harb. Perspect. Biol.* 5:a017459
102. Choi E, Yu H. 2018. Spindle checkpoint regulators in insulin signaling. *Front. Cell Dev. Biol.* 6:161
103. Carpentier JL. 1994. Insulin receptor internalization: molecular mechanisms and physiopathological implications. *Diabetologia* 37(Suppl. 2):S117–24

104. Fagerholm S, Ortegren U, Karlsson M, Ruishalme I, Stralfors P. 2009. Rapid insulin-dependent endocytosis of the insulin receptor by caveolae in primary adipocytes. *PLOS ONE* 4:e5985
105. Backer JM, Kahn CR, Cahill DA, Ullrich A, White MF. 1990. Receptor-mediated internalization of insulin requires a 12-amino acid sequence in the juxtamembrane region of the insulin receptor β-subunit. *J. Biol. Chem.* 265:16450–54
106. Backer JM, Shoelson SE, Haring E, White MF. 1991. Insulin receptors internalize by a rapid, saturable pathway requiring receptor autophosphorylation and an intact juxtamembrane region. *J. Cell Biol.* 115:1535–45
107. Tang R, Jiang Z, Chen F, Yu W, Fan K, et al. 2020. The kinase activity of *Drosophila* BubR1 is required for insulin signaling-dependent stem cell maintenance. *Cell Rep.* 31:107794
108. Choi E, Kikuchi S, Gao H, Brodzik K, Nassour I, et al. 2019. Mitotic regulators and the SHP2-MAPK pathway promote IR endocytosis and feedback regulation of insulin signaling. *Nat. Commun.* 10:1473
109. Caro JF, Ittoop O, Pories WJ, Meelheim D, Flickinger EG, et al. 1986. Studies on the mechanism of insulin resistance in the liver from humans with noninsulin-dependent diabetes. Insulin action and binding in isolated hepatocytes, insulin receptor structure, and kinase activity. *J. Clin. Investig.* 78:249–58
110. Soll AH, Kahn CR, Neville DM Jr. 1975. Insulin binding to liver plasma membranes in the obese hyperglycemic (*ob/ob*) mouse. Demonstration of a decreased number of functionally normal receptors. *J. Biol. Chem.* 250:4702–7
111. Howard JK, Flier JS. 2006. Attenuation of leptin and insulin signaling by SOCS proteins. *Trends Endocrinol. Metab.* 17:365–71
112. Song R, Peng W, Zhang Y, Lv F, Wu HK, et al. 2013. Central role of E3 ubiquitin ligase MG53 in insulin resistance and metabolic disorders. *Nature* 494:375–79
113. Yi JS, Park JS, Ham YM, Nguyen N, Lee NR, et al. 2013. MG53-induced IRS-1 ubiquitination negatively regulates skeletal myogenesis and insulin signalling. *Nat. Commun.* 4:2354
114. Nagarajan A, Petersen MC, Nasiri AR, Butrico G, Fung A, et al. 2016. MARCH1 regulates insulin sensitivity by controlling cell surface insulin receptor levels. *Nat. Commun.* 7:12639
115. Carracedo A, Pandolfi PP. 2008. The PTEN–PI3K pathway: of feedbacks and cross-talks. *Oncogene* 27:5527–41
116. Clement S, Krause U, Desmedt F, Tanti JF, Behrends J, et al. 2001. The lipid phosphatase SHIP2 controls insulin sensitivity. *Nature* 409:92–97
117. Lazar DF, Saltiel AR. 2006. Lipid phosphatases as drug discovery targets for type 2 diabetes. *Nat. Rev. Drug Discov.* 5:333–42
118. Anderie I, Schulz I, Schmid A. 2007. Direct interaction between ER membrane-bound PTP1B and its plasma membrane-anchored targets. *Cell Signal.* 19:582–92
119. Popov D. 2012. Endoplasmic reticulum stress and the on site function of resident PTP1B. *Biochem. Biophys. Res. Commun.* 422:535–38
120. Issad T, Boute N, Boubekeur S, Lacasa D. 2005. Interaction of PTPB with the insulin receptor precursor during its biosynthesis in the endoplasmic reticulum. *Biochimie* 87:111–16
121. Soos MA, Siddle K. 1989. Immunological relationships between receptors for insulin and insulin-like growth factor I. Evidence for structural heterogeneity of insulin-like growth factor I receptors involving hybrids with insulin receptors. *Biochem. J.* 263:553–63
122. Moxham CP, Duronio V, Jacobs S. 1989. Insulin-like growth factor I receptor β-subunit heterogeneity. Evidence for hybrid tetramers composed of insulin-like growth factor I and insulin receptor heterodimers. *J. Biol. Chem.* 264:13238–44
123. Soos MA, Whittaker J, Lammers R, Ullrich A, Siddle K. 1990. Receptors for insulin and insulin-like growth factor-I can form hybrid dimers. Characterisation of hybrid receptors in transfected cells. *Biochem. J.* 270:383–90
124. Bailyes EM, Nave BT, Soos MA, Orr SR, Hayward AC, Siddle K. 1997. Insulin receptor/IGF-I receptor hybrids are widely distributed in mammalian tissues: quantification of individual receptor species by selective immunoprecipitation and immunoblotting. *Biochem. J.* 327(Part 1):209–15
125. Pandini G, Frasca F, Mineo R, Sciacca L, Vigneri R, Belfiore A. 2002. Insulin/insulin-like growth factor I hybrid receptors have different biological characteristics depending on the insulin receptor isoform involved. *J. Biol. Chem.* 277:39684–95

126. Xu Y, Margetts MB, Venugopal H, Menting JG, Kirk NS, et al. 2022. How insulin-like growth factor I binds to a hybrid insulin receptor type 1 insulin-like growth factor receptor. *Structure* 30:1098–108.e6
127. Xu Y, Kirk NS, Venugopal H, Margetts MB, Croll TI, et al. 2020. How IGF-II binds to the human type 1 insulin-like growth factor receptor. *Structure* 28:786–98.e6
128. Zhang X, Yu D, Sun J, Wu Y, Gong J, et al. 2020. Visualization of ligand-bound ectodomain assembly in the full-length human IGF-1 receptor by cryo-EM single-particle analysis. *Structure* 28:555–61.e4
129. Bai XC. 2021. Seeing atoms by single-particle cryo-EM. *Trends Biochem. Sci.* 46:253–54
130. Yamada K, Goncalves E, Kahn CR, Shoelson SE. 1992. Substitution of the insulin receptor transmembrane domain with the c-neu/erbB2 transmembrane domain constitutively activates the insulin receptor kinase in vitro. *J. Biol. Chem.* 267:12452–61
131. Cheatham B, Shoelson SE, Yamada K, Goncalves E, Kahn CR. 1993. Substitution of the erbB-2 oncoprotein transmembrane domain activates the insulin receptor and modulates the action of insulin and insulin-receptor substrate 1. *PNAS* 90:7336–40
132. McMahon C, Baier AS, Pascolutti R, Wegrecki M, Zheng S, et al. 2018. Yeast surface display platform for rapid discovery of conformationally selective nanobodies. *Nat. Struct. Mol. Biol.* 25:289–96
133. Bai XC, Rajendra E, Yang G, Shi Y, Scheres SH. 2015. Sampling the conformational space of the catalytic subunit of human γ-secretase. *eLife* 4:e11182
134. Denisov IG, Sligar SG. 2016. Nanodiscs for structural and functional studies of membrane proteins. *Nat. Struct. Mol. Biol.* 23:481–86
135. Frauenfeld J, Loving R, Armache JP, Sonnen AF, Guettou F, et al. 2016. A saposin-lipoprotein nanoparticle system for membrane proteins. *Nat. Methods* 13:345–51
136. Carlson ML, Young JW, Zhao Z, Fabre L, Jun D, et al. 2018. The Peptidisc, a simple method for stabilizing membrane proteins in detergent-free solution. *eLife* 7:e34085
137. Michailidis IE, Rusinova R, Georgakopoulos A, Chen Y, Iyengar R, et al. 2011. Phosphatidylinositol-4,5-bisphosphate regulates epidermal growth factor receptor activation. *Pflugers Arch.* 461:387–97
138. Virkamaki A, Ueki K, Kahn CR. 1999. Protein–protein interaction in insulin signaling and the molecular mechanisms of insulin resistance. *J. Clin. Investig.* 103:931–43
139. Turk M, Baumeister W. 2020. The promise and the challenges of cryo-electron tomography. *FEBS Lett.* 594:3243–61
140. Jumper J, Evans R, Pritzel A, Green T, Figurnov M, et al. 2021. Highly accurate protein structure prediction with AlphaFold. *Nature* 596:583–89